Onset of current self-quenching in a metal/CdS/LaS cold cathode in the presence of inelastic scattering in the CdS layer

Yamini Modukuru and Marc Cahay[a)]
Department of Electrical Engineering, University of Cincinnati, Cincinnati, Ohio 45221

Heidrun Kolinsky
Physikalisches Institut, Universität Bayreuth, D-95440 Bayreuth, Germany

Philip Mumford
Air Force Research Laboratory, Sensors Directorate, Wright–Patterson Air Force Base, Dayton, Ohio 45433

(Received 1 November 1999; accepted for publication 4 January 2000)

We use an ensemble Monte-Carlo approach to analyze the importance of space-charge effects in the cathode to anode gap region of a recently proposed metal/CdS/LaS cold cathode and its influence on the energy distribution of the electrons collected at the anode. Our analysis is based on a mean-free path approach to include the effects of inelastic scattering in the CdS layer following Fowler–Nordheim injection across the metal/CdS interface. We investigate in detail the regime of current self-quenching and show the importance of the effects of space charge in narrowing the energy of the electron beam collected at the anode. We compare our results to an analytical treatment of the current self-quenching regime based on a hydrodynamic description of electron transport through the gap. © *2000 American Institute of Physics.* [S0021-8979(00)04807-6]

I. IMPORTANCE OF SPACE-CHARGE EFFECTS

Recently[1] we analyzed the importance of space-charge effects in the cathode to anode gap region of a metal/CdS(cadmium sulfide)/LaS (lanthanum sulfide) cold cathode.[2,3] The main elements in the design and functioning of the emitter are (1) a wide band gap semiconductor (undoped CdS) sandwiched between a metallic contact that supplies electrons into the CdS conduction band at a sufficient rate and (2) a thin semimetallic film that facilitates coherent transport (tunneling) of electrons from the semiconductor conduction band into vacuum.

This injection of electrons into vacuum becomes possible and is effective as long as the semimetallic film is very thin and has a work function low enough that its vacuum edge is located energetically below the conduction band edge of the semiconductor. This situation is referred to as *negative electron affinity*.[4] In the past, we have modeled the transport of electrons between the LaS surface and the anode contact taking into account the energy distribution of carriers due to Fowler–Nordheim injection in the active portion of the cold cathode, assuming ballistic transport across the CdS and LaS layers. The effects of shot noise in the injection current were included in the simulations. Details of the simulations are described in Ref. 1.

As illustrated in Fig. 1, one important feature of transport in the vacuum air gap between the cathode and the anode is that electrons are injected with a finite velocity much in excess of the thermal velocity of thermionic cathodes. At high injection current density, space-charge effects lead to current self-quenching and the anode conduction current is much smaller than the Fowler–Nordheim injected current. However, the limiting value of the measured average anode current density is much larger than the Child–Langmuir limit.[1] In this current self-quenching regime, we have shown in the past that the chopping action of the beam is sometimes accompanied by high-frequency (several tens of GHz) fluctuation in the minimum of the electrostatic potential in the air gap (see Fig. 1). These oscillations lead to large oscillations in the anode current.[1]

In this article, we investigate in further detail the chopping action of the electrostatic potential in front of the cathode and its effect on the energy spread of the carriers collected at the anode. As it turns out, the chopping action of the beam is quite substantial, leading to an energy spread at the anode with a full width at half maximum of only a few k_BT. This is important for practical applications such as flat panel displays or traveling wave tubes which require electron beams that are as monoenergetic as possible.[5] Our analysis includes the effects of inelastic scattering in the CdS layer. Recently, Kolinsky and Schamel[6,7] used a hydrodynamic Lagrangian description to derive analytical expressions of the space-charge-limited current in pure electron diodes for arbitrary potential across the gap between the cathode and the anode. For electron beams injected at the cathode with a fixed velocity v_0 and negligible energy spread, they derived analytical expressions for the minimum current necessary for the existence of a virtual cathode solution and for the transmitted current as a function of the injected current for a given cathode to anode separation and bias across the gap. Hereafter, we compare the results of our ensemble Monte-Carlo (EMC) simulations to the results of the analytical treatment of Kolinsky and Schamel.

a)Electronic mail: mcahay@planck.ececs.uc.edu

 © 2000 American Institute of Physics

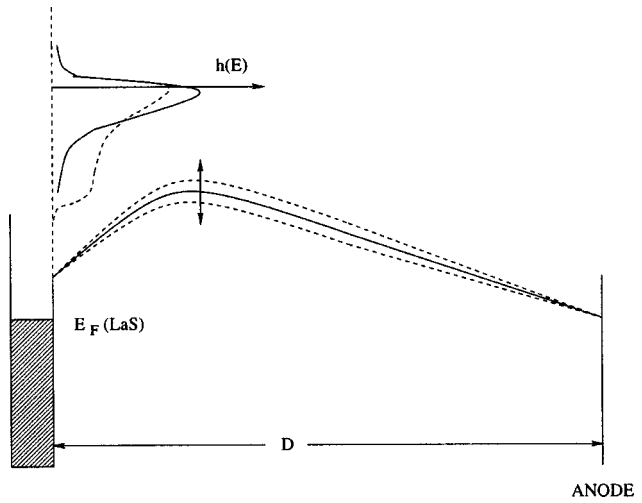

FIG. 1. Illustration of the chopping action of the electrostatic potential energy profile in front of the LaS thin film as a result of the space-charge effects in the cathode to anode region. The energy distribution $h(E)$ of the current injected into vacuum is shown under the approximation of ballistic transport (solid line) and for the case of inelastic scattering in the CdS layer (dashed line). In the current self-quenching regime, the potential energy profile can oscillate rapidly in front of the cathode (shown by vertical arrows) and the average current collected at the anode is much smaller than the injected current.

This article is organized as follows. In Sec. II, we briefly describe the EMC simulator used to study the space-charge effects mentioned above. The effects of inelastic scattering in the CdS layer are included using a mean-free path approach.[8] In Sec. III, we present numerical simulations for the average anode current versus injection current from the metal/CdS/LaS cold cathode as a function of the electron mean-free path in the CdS layer. We compare the energy profile of the current collected at the anode and the energy distribution of the current injected at the cathode as a function of the biasing point in the current self-quenching regime. We also compare our results for the (time) average anode current with the predictions of Kolinsky, and Schamel based on the assumption of monoenergetic beam injection.[6,7] In Sec. IV we give our conclusions.

II. APPROACH

Details of the EMC simulator to describe space-charge effects in the cathode to anode region following Fowler–Nordheim injection from the metal/CdS/LaS cold cathode are given in Ref. 1. We will briefly summarized the technique.

First, we use a flux method to calculate the energy spectrum of the electron flux injected into the CdS following Fowler–Nordheim (FN) tunneling injection at the metal/CdS interface. More specifically, we calculate the energy dependence of the function $h(E)$ defined as the total energy distribution for emitted electrons or the differential current density divided by the electronic charge e, i.e.,

$$J_{\mathrm{FN}} = e \int_0^{+\infty} h(E)\,dE, \tag{1}$$

where J_{FN} is the Fowler–Nordheim emission current and E is the total energy of the electron. In the case of ballistic transport through the CdS and LaS regions and if we assume perfect transmission (equal to unity for all electrons) at the CdS/LaS and LaS/vacuum interfaces, the flux $h(E)$ can then be used as an initial electron energy distribution to simulate electron injection through the space-charge region between the LaS thin film and the anode. In the case of Fowler–Nordheim injection, assumed here, an expression for $h(E)$ was derived in Ref. 1.

Once the injected energy distribution $h(E)$ as a function of the applied bias across the CdS layer has been found in order to include the effects of shot noise in the Fowler–Nordheim emitter current, we must estimate (1) the number of electrons emitted in each time interval, (2) the times at which the electrons are emitted, and (3) the initial velocities of the electrons. The simulation proceeds as follows: (1) First, the emitted current density is determined as a function of applied bias across the CdS layer for a specific set of cathode parameters using a semi analytical treatment,[2] (2) the energy spectrum $h(E)$ of the injected carriers is then determined. Next, the EMC simulation of electron transport through the air gap between the LaS thin film and the anode is run as follows: (1) The simulation time is divided into small intervals (selected to be 50 fs in our simulations) after which the conduction band energy profile between the LaS emitting surface and the anode thin film is upgraded through solution of the Poisson equation. The boundary conditions used to solve the Poisson equation are the predetermined fixed values of the electrostatic potential applied at the LaS thin film and anode material.[1] (2) Electrons which are reflected towards the cathode (LaS thin film) as a result of the conduction band maximum in front of the cathode and cross the LaS surface with a negative velocity are automatically removed from the simulation. Similarly, electrons crossing the plane of the anode are also assumed to be absorbed and therefore removed from the simulation.

A. Effects of shot noise

Electrons escape from the contact randomly in time and with a distribution of velocities. The aggregate of emitted electrons contains current fluctuations, due to the random emission times, and velocity (and therefore energy) fluctuations, since the number of electrons in any small range of energies within the distribution also fluctuates as a consequence of the random emission times. By random emission, we mean simply that the emission of every electron is completely independent of every other electron emission. We describe such a random process by assuming that the number of electrons emitted per unit time is given by a Poisson distribution and that their corresponding emission energies are given by the energy distribution density $h(E)$ described above. We must generate a set of numbers which simulates the cathode emission and which possesses all the statistical features of shot noise.[1]

B. Inelastic scattering in the CdS layer

We extend the model described above to include the effects of inelastic scattering in the CdS layer using a mean-

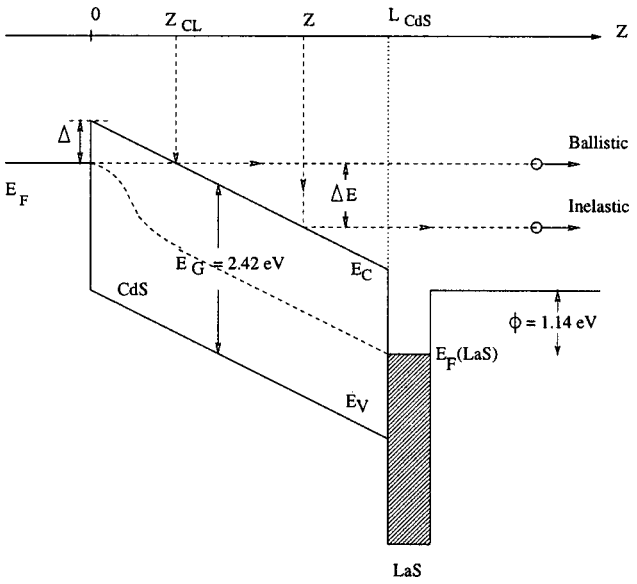

FIG. 2. Illustration of the effects of inelastic scattering in the CdS layer. We use a mean-free path approach to calculate the inelastic component of the current injected into vacuum. Because we neglect electron-hole recombination, the sum of the ballistic and inelastic components of the beam injected into vacuum is equal to the Fowler–Nordheim tunneling current across the metal/CdS interface. z is the randomly selected location where the inelastic scattering event occurs, after which the electron is assumed to drop to the bottom of the conduction band in CdS. Subsequently, that electron is assumed to travel ballistically towards the CdS/LaS interface; z_{cl} is the location of the classical turning point for an electron tunneling from the metal/CdS interface. We neglect inelastic scattering events for z between 0 and z_{cl}. The long-dashed line is a qualitative representation of the variation of the quasi-Fermi level across the CdS region under current injection.

free path concept (see Fig. 2). At a location z in the CdS layer, the ballistic component of the current is approximated as[8]

$$J_z^b = J_{\mathrm{FN}} e^{-z/\lambda \mathrm{Cds}}, \tag{2}$$

where J_{FN} is the Fowler–Nordheim current injected across the metal/CdS interface and λ_{CdS} is the mean-free path in the CdS layer. For simplicity, the latter is assumed to be independent of the applied bias across the CdS layer. In Eq. (2), $z=0$ at the metal/CdS interface. Under steady-state conditions and in the absence of recombination processes,[9] the differential current density loss at z is therefore given by

$$dJ_z^b = -\frac{1}{\lambda_{\mathrm{Cds}}} J_{\mathrm{FN}} e^{-(z/\lambda_{\mathrm{Cds}})} dz. \tag{3}$$

If we make the simplifying assumption that electrons make at most one collision on their travel through the CdS layer,[10] the kinetic energy released by electrons suffering an inelastic collision within the range $(z, z+dz)$ can be easily calculated (See Appendix A).

Hereafter, we assume that the transmission coefficients through the CdS/LaS and LaS/vacuum interfaces is equal to unity. The energy distribution of the electron beam injected into vacuum is then determined as follows. The electrons injected across the metal/CdS interface are randomly selected according to the energy distribution $h(E)$ describing Fowler–Nordheim injection across that interface. Then, the probability of that electron suffering inelastic scattering in the CdS layer is selected according to a probability distribution deduced from Eq. (3). Using a rejection technique, we then allow each electron injected across the (metal/CdS) interface to suffer inelastic scattering by generating a uniform random number r in the [0, 1] interval and checking if

$$z = -\lambda_{\mathrm{Cds}} \log \tau \tag{4}$$

is below L_{CdS}. In addition, we only allow inelastic scattering if z is larger than the classical turning point z_{cl} shown in Fig. 2. This is a simplifying assumption which amounts to neglecting inelastic processes during the tunneling process under the triangular barrier shown in Fig. 2.

As mentioned above, we assume that the electron only suffers one collision in the CdS layer which brings it down to the bottom of the conduction band in the CdS layer, after which the electron moves ballistically towards the CdS/LaS interface. This is illustrated in Fig. 2. Our model is quite simple but leads to a qualitatively correct energy distribution for the electrons injected into vacuum as shown in the numerical examples below. Our simple model predicts that the beam injected into vacuum has a ballistic component (which is characterized be a fairly narrow energy beam) and a long tail extending towards low energy whose intensity increases as the mean-free path in the CdS layer is decreased. Detailed results of numerical simulations are described in Sec. III.

C. Analytical results

In our numerical simulations, we will compare the EMC values for the anode current in the current self-quenching regime to the results predicted from the well-known Child–Langmuir result.[11,12] The latter is strictly valid for thermionic cathodes with a planar geometry. For a cathode to anode gap separation D and gap voltage V_{gap}, the maximum electron current density allowed for time-independent flow solution is given by[11,12]

$$J_{CL} = \frac{4\epsilon_0}{9D^2} \sqrt{\frac{2e}{m}} V_{\mathrm{gop}}^{3/2}, \tag{5}$$

where e and m are, respectively, the charge and mass of the free electron, and ϵ_0 is the free space permittivity. J_{CL} is also called the limiting current density or critical current density. In the current self-quenching regime, an anode current in excess to the Child–Langmuir limit is expected since the latter is based on the assumption of zero electron emission velocity, which is not the case for the cold cathode considered here as illustrated below.

A thorough extension of the Child–Langmuir theory for planar diodes for the case of electron beam injection with finite velocity v_{inj} was recently developed by Kolinsky and Schamel.[6,7] They showed that the threshold for the injection current at which current self-quenching occurs is given by

$$J_{\mathrm{th}} = F(X) J_{CL}, \tag{6}$$

where

$$F(X) = \left(\frac{1+\sqrt{1+X}}{\sqrt{X}} \right)^3, \tag{7}$$

TABLE I. Material parameters of the cold cathode.

Material	Au	*i*-CdS	LaS
Lattice thickness (Å)	Optional	75.0	24.6
Lattice constant (Å)	4.04	5.83	5.85
Work function (eV)	4.3	4.2	1.14
Band gap (eV)		2.5	
No. of free electrons ($10^{22}\,\mathrm{cm}^{-3}$)	(5.86)	⋯	1.99
Electron mass (m_0)	1.0	0.14	1.0

where $X = eV_{\mathrm{gap}}/0.5 m_0 v_{\mathrm{inj}}^2$, V_{gap} being the voltage across the gap, m_0 the free electron mass, and v_{inj} the velocity of the electron injected into vacuum. Hereafter, we calculate v_{inj} starting with $0.5\, m_0 v_{\mathrm{inj}}^2 = E_{\mathrm{peak}}$, where E_{peak} is the peak location of the energy distribution $h(E)$ of injected carriers.

In this formalism, the collected anode J_A current past the threshold is given by

$$J_A = \eta J_{\mathrm{FN}}, \tag{8}$$

where η is the transmitted fraction of the injected current J_{FN}. The coefficient η has a fairly complicated analytical expression and is given in Appendix B for the sake of completeness.

III. NUMERICAL RESULTS

We consider a specific cathode with the parameters listed in Table I. In all simulations, the spacing between the LaS thin film and the anode is set equal to 15 μm and the width of the CdS layer is set equal to 75 Å. We consider a cold cathode with a Au/CdS interface for which Δ is equal to 0.78 eV.[13] The simulation domain is divided into 300 bins of 500 Å each. This is the length traveled by an electron with a velocity of 10^8 cm/s over a period of 50 fs, the time interval at which we upgrade the Poisson solver. To make the EMC simulator more efficient, the bin size was selected so that electrons could not cross several bins between solutions of the Poisson solver. To calculate the steady-state value of the anode current, the EMC simulations are run for 20 000 time steps (1 ns). As shown in Fig. 15 of Ref. 1, when current self-quenching occurs, the anode current can contain an ac component of large frequency (several tens of GHz) equal to the chopping frequency of the electrostatic potential maximum in front of the cathode. In this case, the anode current and the energy spread of the electrons collected at the anode shown below are calculated while averaging over many oscillations of the ac signal (the average is carried over the final 1000 and 500 time steps of the EMC simulations to calculate the average anode current and distribution of collected carriers, respectively).

We summarize the onset of current self-quenching in Figs. 3 and 4 for a bias between a cathode and an anode equal to 1 and 5 V, respectively. In Figs. 3 and 4, the curves labeled with a value of λ are the results of our EMC simulator for different values of the inelastic mean-free path in the CdS layer. The curve labeled **ballistic** corresponds to an infinite mean-free path in the CdS layer (ballistic transport). The bottom dashed line is the Child–Langmuir result. For

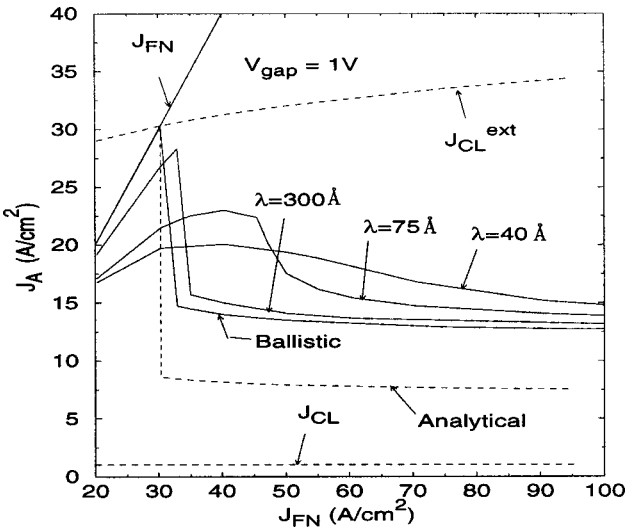

FIG. 3. Time average of the conduction current density in the rightmost bin of the simulation vs injection current density. The bias across the cathode to anode gap is equal to 1 V. The bottom dashed line is the Child–Langmuir result. The top dashed line is the extended Child–Langmuir limit based on the assumption of injection into vacuum at a finite velocity [Eq. (8)]. The curves labeled with different values of λ are the results of the ensemble Monte-Carlo simulator using different values of the electron mean-free path in the CdS layer. The curve labeled **ballistic** assumes an infinite mean-free path in CdS. The curve labeled **analytical** is the theoretical hydrodynamic model described in detail in Refs. 6 and 7.

$V_{\mathrm{gap}} = 1$ and 5 V, Eq. (5) gives J_{CL} equal to 1 and 11 A/cm^2, respectively. In Figs. 3 and 4, the curve labeled **analytical** is the result of the theoretical result [Eq. (8)] of Refs. 6 and 7 based on the assumption of injection into vacuum at a finite velocity. In that case, we use the velocity corresponding to the maximum of the energy density flux $h(E)$ of the electron beam injected into vacuum. This velocity varies with the bias across the CdS layer. The top dashed curves in Figs. 3 and 4 are the extended Child–Langmuir results [Eq. (6)].

As seen in Figs. 3 and 4, the prediction for the threshold to the current self-quenching regime (i.e., when $J_A < J_{\mathrm{FN}}$) is

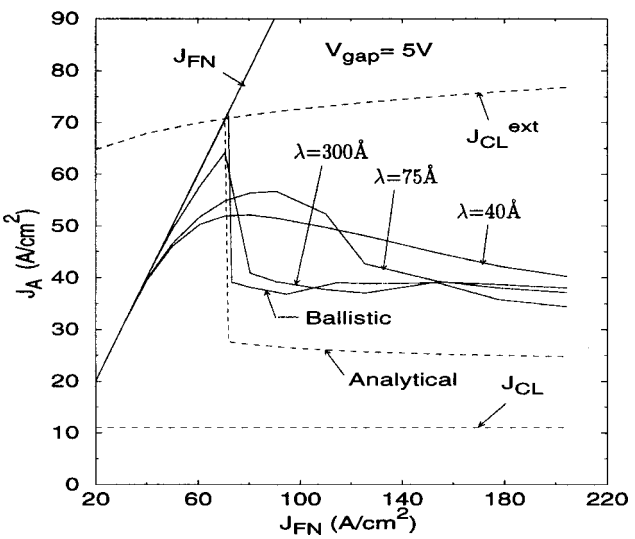

FIG. 4. Same as Fig. 3 for a bias across the cathode to anode gap equal to 5 V.

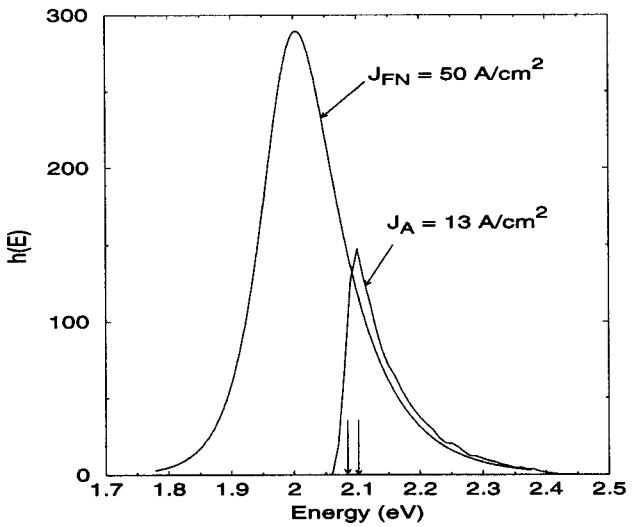

FIG. 5. Plot of the energy density flux of the electron beam injected into vacuum ($J_{FN}=50$ A/cm^2) and electron beam collected at the anode, J_A. The latter represents the energy distribution of carriers collected at the anode over a period corresponding to the last 500 time steps of the EMC simulations. The two vertical arrows show the extremum values of the maximum of the fluctuating electrostatic potential energy profile in the gap. The zero of energy is the vacuum level outside the LaS thin film. The anode energy flux density has been shifted downward in energy by an amount equal to eV_{gap} (with $V_{gap}=1$ eV).

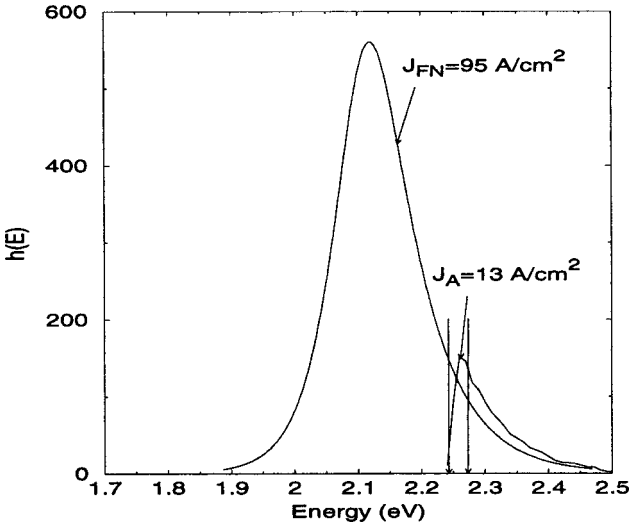

FIG. 6. Same as Fig. 5 for $J_{FN}=95$ A/cm^2.

quite accurately predicted by Eq. (6) under the assumption of ballistic transport through the CdS layer. In this case, the EMC results for the current collected at the anode are larger than predicted in the theoretical hydrodynamic model.[6,7] This point will be addressed in detail below. When inelastic processes using an electron mean-free path approach are included, the transition to the regime of current self-quenching is more gradual as the mean-free path decreases. Furthermore, past the threshold, the anode current is larger than in the ballistic case.

A. Ballistic regime

In order to understand why the EMC J_A results are larger than the analytical results, we plot in Figs. 5 and 6 the energy flux distribution of the injected electrons and electrons collected at the anode for two different values of the injected current density J_{FN} (for the case of $V_{gap}=1$ V). One value corresponds to a biasing point right after the threshold for self-quenching is reached (Fig. 5), and the other is well into the self-quenching regime (Fig. 6).

In Figs. 5 and 6, the energy distribution is the energy distribution of carriers collected over a period corresponding to the last 500 time steps (25 ps) of the EMC simulations. The areas under the curves in Figs. 5 and 6 are proportional to the injected current (J_{FN}) and average anode current (J_A) collected at the anode. For the energy flux density collected at the anode, the distribution has been shifted down in energy by an amount equal to eV_{gap} (with $V_{gap}=1$ V) to stress the chopping action of the electrostatic potential in front of the cathode, the zero of energy being the vacuum level right outside the LaS thin film. In Figs. 5 and 6 we show with vertical arrows the minimum and maximum values of the electrostatic potential energy in the gap. These values are above the location of the maxima of the energy flux density of the injected beam. Both Figs. 5 and 6 indicate that a substantial fraction of the beam is cross the gap with energy above the maximum of the electrostatic potential energy. This explains why the EMC results predict a larger anode current value than the analytical treatment which assumes injection of the carriers at an energy corresponding to the peak of the injected distribution. In Figs. 5 and 6, we also note that some electrons are collected at the anode with a kinetic energy below the minimum value of the electrostatic potential in front of the cathode. This is due to the time dependence of the electrostatic potential in the gap which allows the total energy of some electrons to decrease while crossing the gap. Simultaneously, some electrons can gain

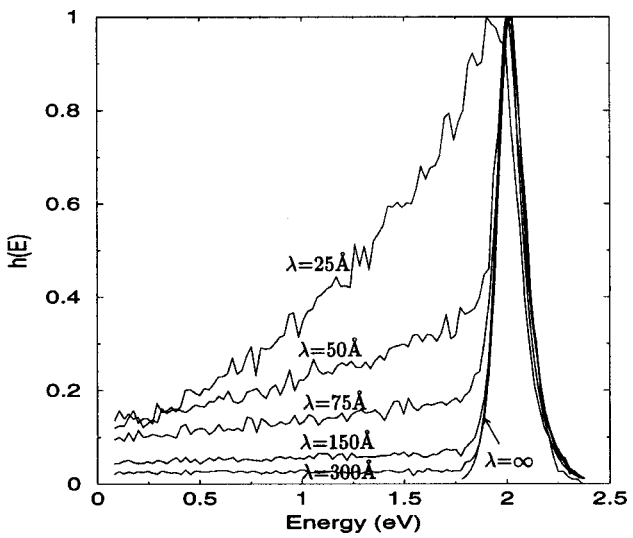

FIG. 7. Plot of the energy flux density of the injected beam for $J_{FN}=50$ A/cm^2 for different values of the mean-free path λ_{CdS} in the CdS layer. The zero of energy is the vacuum level outside the LaS thin film. The increase in the inelastic portion of the injected beam is readily seen for smaller λ_{CdS}. The abrupt cutoff at low energy corresponds to electrons at the bottom of the conduction band in CdS at the CdS/LaS interface.

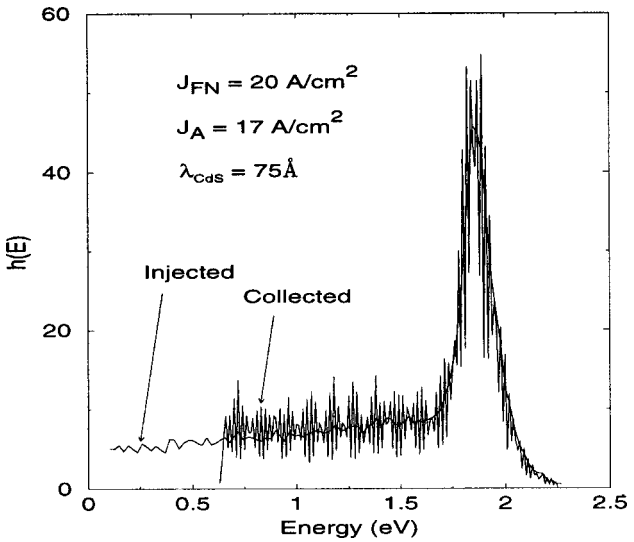

FIG. 8. Plot of the injected and collected energy density flux for $J_{FN}=20$ A/cm^2. The anode energy flux density has been shifted downward in energy by an amount equal to eV_{gap} ($V_{gap}=1$ eV). The mean-free path λ_{CdS} is set equal to 75 Å.

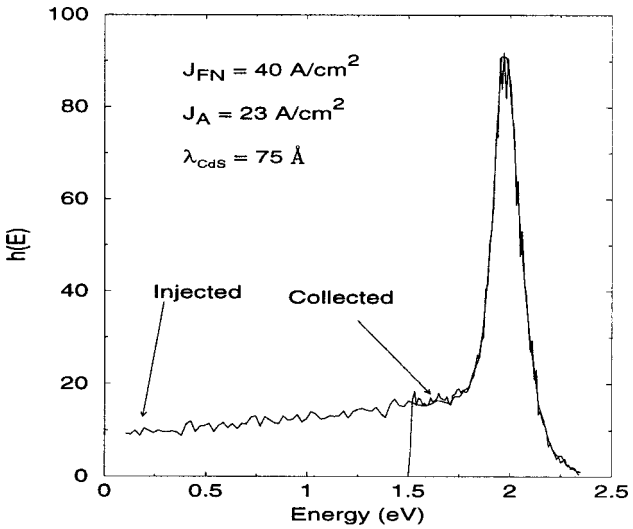

FIG. 9. Same as Fig. 8 for $J_{FN}=40$ A/cm^2.

energy while crossing the gap which explains why the upper tail of the energy flux collected at the anode is larger than the upper tail of the injected distribution.

B. Effects of inelastic scattering

We first show in Fig. 7 the effects of inelastic scattering in the CdS layer on the energy distribution of the injected carriers for different values of the electron mean-free path λ_{CdS}. In Fig. 7, the different curves represent the energy flux density corresponding to an injection current $J_{FN}=50$ A/cm^2 for different λ_{CdS}. Because we neglect the effects of recombination in the CdS layer, the area under each curve is the same (the zero of energy is the vacuum level right outside the LaS thin film). Figure 7 shows the expected larger contribution to the tail of the distribution at lower energy for shorter mean-free paths in the CdS layer. The abrupt cut of the tail at low energy corresponds to electrons located at the minimum of the conduction band in the CdS layer at the CdS/LaS interface.

As a result of the tail at low energy in the presence of inelastic scattering, we expect the chopping action of the electrostatic potential in front of the cathode to be effective at a lower value of the injected current density J_{FN}. This explains why the effects of current self-quenching occur at lower values of J_{FN} in both Figs. 5 and 6, compared to the threshold observed under the assumption of ballistic transport. For a given bias across the gap, the current self-quenching regime also appears at a lower value of the injected current density for a larger electron mean-free path in the CdS layer since the tail of the inelastic portion of the injected beam extends to lower energy.

Since the energy distribution of the injected carriers is more spread in energy in the presence of inelastic scattering in the CdS layer, we expect the chopping action of the electrostatic potential to be more gradual as the injected current density increases, leading to a smoother transition to the regime of current self-quenching. The transition is increasingly smoother as the mean-free path is getting shorter and shorter, as shown in Figs. 5 and 6.

Finally, we show in Figs. 8–11 the gradual chopping action of the electrostatic potential in the gap on the energy flux density collected at the anode as a function of the injected current density (for the case of $V_{gap}=1$ V and $\lambda_{CdS}=75$ Å). Even though not shown here, a similar trend was observed for the case of $V_{gap}=5$ V. In Figs. 8–11, we also show the energy flux density of the injected beam. Figure 3 shows that the anode current is roughly constant for injected current densities in excess of 50 A/cm^2. Figures 8–11, however, indicate that the energy spread of the beam collected at the anode gets increasingly narrower when the cathode is operated further into the current self-quenching regime (larger J_{FN}). This would be the favored mode of operation of the cathode for applications requiring an electron beam as narrow as possible, like in traveling wave tubes. Figure 11

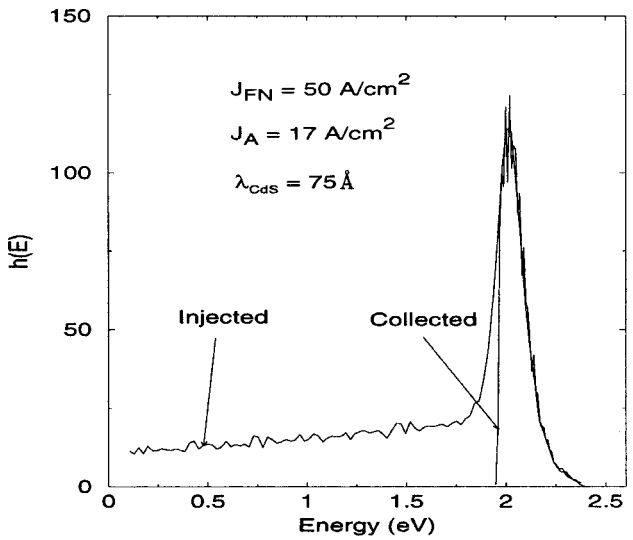

FIG. 10. Same as Fig. 8 for $J_{FN}=50$ A/cm^2.

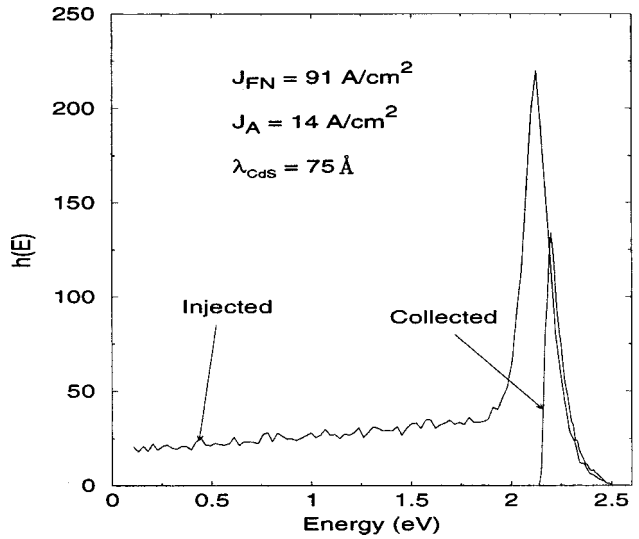

FIG. 11. Same as Fig. 8 for $J_{FN}=90$ A/cm^2.

shows that the full width at half maximum of the beam is about 100 meV, which is about $4k_BT$ at room temperature.

IV. CONCLUSIONS

We have used an ensemble Monte-Carlo approach to analyze the importance of space-charge effects in the cathode to anode gap region of a recently proposed metal/CdS/LaS cold cathode and its influence on the energy distribution of the electrons collected at the anode. Our analysis is based on a mean-free path approach to include the effects of inelastic scattering in the CdS layer following Fowler–Nordheim injection across the metal/CdS interface. After the onset of current self-quenching, the energy spread of the electron beam collected at the anode is substantially narrower than it is for the beam injected from the cathode into vacuum due to chopping of the beam by oscillations of the electrostatic potential in front of the cathode. Under the approximation of ballistic transport through the CdS layer, the value of the cathode injection current at which the onset of current self-quenching occurs is in very good agreement with the results of a theoretical hydrodynamic description of electron transport across the gap under the assumption of electron injection from the cathode at a finite velocity. In the current self-quenching regime, our Monte-Carlo simulations predict a larger anode current than the theoretical cold fluid model due to the energy spread of the injected energy distribution. When the effects of inelastic scattering through the CdS layer are included, the transition to the regime of current self-quenching (i.e., a drop in the anode current as a function of the injection current) is more gradual compared to the case of ballistic transport through the CdS layer.

ACKNOWLEDGMENTS

Two of the authors (M.C. and Y.M.) acknowledge the support of the National Science Foundation under Award No. ECS-9632511. This work was also supported by the Air Force Research Laboratory, Sensors Directorate, Wright–Patterson Air Force Base, under Contract No. F33615-98-C-1204. One author (Y.M.) was partially supported by a summer research fellowship from the University of Cincinnati Research Council.

APPENDIX A

For an electron tunneling through the Au/CdS interface with an energy equal to the Fermi level in the metallic contact, the energy loss ΔE in the CdS layer (see Fig. 2) is easily found by using the law of congruent triangles,

$$\frac{\Delta + eV_{\text{bias}} - 0.5E_G}{\Delta E + \Delta} = \frac{L_{\text{Cds}}}{z}, \tag{A1}$$

where z is the location where the electron loses its energy, e is the charge of the electron, Δ is the height of the barrier at the Au/CdS interface, and V_{bias} is the applied potential across the CdS layer.

Rearranging Eq. (A1), we obtain

$$\Delta E = eV_{\text{bias}} pz/L_{\text{CdS}} - \Delta, \tag{A2}$$

where

$$p = 1 + \frac{\Delta - 0.5E_G}{eV_{\text{bias}}}. \tag{A3}$$

For an electron incident with an energy different from the Fermi level in the Au contact, a similar procedure can be used to find the corresponding energy loss in the CdS layer. This technique is used in the Monte-Carlo approach in Sec. II to determine the distribution of the carriers injected into vacuum at the CdS/LaS interface.

APPENDIX B

In the theoretical treatment used in Refs. 6 and 7, the fraction of the injected current collected at the anode in the current self-quenching regime under the assumption of carrier injection at a specific velocity (v_{inj}) is given by

$$\eta = \frac{2\nu}{1+\nu}, \tag{B1}$$

where

$$\nu = \frac{(2V+1)^{3/2}}{(1-1/x^*)^2}, \tag{B2}$$

and

$$V = \frac{eV_{\text{bias}}}{m_e v_{\text{inj}}^2}, \tag{B3}$$

where m_e is the free electron mass.

Furthermore, the following quantities have been introduced:

$$x^* = \frac{6}{\left(3 + \sqrt{d_1} + \sqrt{2c_1 - c_2 - c_3 - 54\dfrac{(C+9\beta^2)}{\sqrt{d_1}}}\right)} \tag{B4}$$

which represents the position of the virtual cathode normalized to the separation D between the cathode and the anode. The following abbreviations have been used:

$$d_1 = c_1 + c_2 + c_3, \tag{B5}$$

where

$$c_1 = -6f + 9, \tag{B6}$$

$$c_2 = 9b^{1/3}, \tag{B7}$$

$$c_3 = f^2 b^{-1/3}, \tag{B8}$$

$$b = a_1 + \tfrac{2}{3}\sqrt{a_2}, \tag{B9}$$

$$a_1 = \tfrac{1}{27} f^3 + 18C\beta^2, \tag{B10}$$

$$a_2 = 3f\beta^2(f^3 + 243C\beta^2), \tag{B11}$$

$$f = C + 1 - 9\beta^2, \tag{B12}$$

$$C = (2V + 1)^{3/2}, \tag{B13}$$

and the normalized injection parameter β is given by

$$\beta = \sqrt{\frac{e^2 n_0}{\epsilon_0 m_e}} \frac{D}{v_{\text{inj}}}. \tag{B14}$$

[1] P. D. Mumford and M. Cahay, J. Appl. Phys. **84**, 2754 (1998).
[2] P. D. Mumford and M. Cahay, J. Appl. Phys. **79**, 2176 (1996).
[3] P. D. Mumford and M. Cahay, J. Appl. Phys. **81**, 3707 (1997).
[4] P. R. Bell, *Negative Electron Affinity Devices* (Clarendon, Oxford, 1973).
[5] S. Iannazzo, Solid-State Electron. **36**, 301 (1993).
[6] H. Kolinsky and H. Schamel, J. Plasma Phys. **57**, 403 (1997).
[7] H. Kolinsky, Ph.D. thesis, Universität Bayreuth, Germany, 1998.
[8] A. Malhotra, Y. Modukuru, and M. Cahay, J. Vac. Sci. Technol. B **16**, 3086 (1998).
[9] In this article, the CdS layer is assumed to be intrinsic. However, real undoped semi-insulating CdS is mostly an *n*-type compensated semiconductor that has traps and recombination centers. The trapping of electrons by these traps may generate space-charge effects which could influence the electron flow through the layer. This possibility would require further analysis. The effects of space charge may not be too dramatic if the CdS layer is thin enough, as assumed here.
[10] Our mean-free path approach is a simplified representation of the actual inelastic processes in the CdS layer. A more careful analysis would require an ensemble Monte-Carlo description of electron transport involving the various scattering mechanisms (phonon, intervalley scattering, etc.) in the CdS layer. Qualitatively, we expect the energy distribution of the carriers injected into vacuum in this refined treatment to also show a ballistic and a low energy tail component as obtained in our simple treatment.
[11] C. D. Child, Phys. Rev. **32**, 492 (1911).
[12] I. Langmuir, Phys. Rev. **21**, 419 (1923).
[13] S. M. Sze, *Physics of Semiconductor Devices*, 2nd ed. (Wiley, New York, 1981), p. 219.